Contents lists available at ScienceDirect

Chemical Engineering Research and Design

journal homepage: www.elsevier.com/locate/cherd

Mathematical modeling and process parametric study of CO_2 removal from natural gas by hollow fiber membranes

Yunhan Chu, Arne Lindbråthen, Linfeng Lei, Xuezhong He, Magne Hillestad**

Department of Chemical Engineering, Norwegian University of Science and Technology (NTNU), NO-7491, Trondheim, Norway

ARTICLE INFO

Article history:
Received 13 December 2018
Received in revised form 6 May 2019
Accepted 24 May 2019
Available online 1 June 2019

Keywords:
Hollow fiber membrane
Module design
CO_2 removal
Mathematical modeling
Natural gas

ABSTRACT

Hollow fiber membranes show a great potential in natural gas sweetening by removing CO_2 to meet gas grid specifications. A membrane model with high prediction accuracy is developed to model multicomponent gas transport through hollow fiber modules. The influences of hollow fiber diameter and length, and packing density on module efficiency related to pressure drops in both sides were systematically investigated based on the developed model. The total pressure drop along the length is less than 1% if the inner diameter of hollow fibers (0.6 m length) is larger than 200 μm. Moreover, the highest module packing density was found to be dependent on hollow fiber dimension, and too high packing density will cause extreme high pressure drops. Both feed CO_2 concentration and pressure were found to significantly influence membrane module performance related to the required specific membrane area and hydrocarbon loss based on process parametric study of CO_2 removal from natural gas. Larger pressure drops along fiber length was found for the more-permeable polyimide membranes compared to the less-permeable cellulose acetate and carbon membranes. The developed model can be used for guiding the design of efficient hollow fiber membrane modules and potentially process simulation of membrane gas separation.

1. Introduction

Natural gas is becoming one of the world's primary energy consumption as it is a less carbon intensive energy sources compared to other fossil fuels (Chu and He, 2018). The raw natural gas composition may vary greatly depending on the region/field, which usually contains considerable amount of light and heavy hydrocarbons (HCs), as well as the impurities such as water, H_2S, CO_2, N_2 and helium. Among them, CO_2 as the main impurity needs to be removed to meet the legal requirements and natural gas network grid specifications. Different technologies such as absorption, pressure swing adsorption, membranes have been reported for CO_2 removal from natural gas (He, 2018). Decision on the proper technology for CO_2 removal from natural gas will be dependent on the raw natural gas composition, the process condition and the plant location. Conventional chemical (amine) absorption is well known and implemented in industrial processes, and still considered as the state-of-the-art technology for CO_2 capture. However, the energy consumption and environmental issues related to a second pollution of amine-based solvents directs to the development of novel environmentally friendly and energy efficient separation technologies (Peters et al., 2011; Baker and Lokhandwala, 2008). Compared to conventional separation technique of chemical and physical absorption, membranes have the advantages of small size (footprint), favorable economics, robust and effective performance, simplicity of operation and maintenance (Bernardo and Drioli, 2010), which shows a great potential in natural gas sweetening. The representative commercial suppliers (e.g.,

* *Corresponding authors.*
E-mail addresses: xuezhong.he@ntnu.no (X. He), magne.hillestad@ntnu.no (M. Hillestad).
https://doi.org/10.1016/j.cherd.2019.05.054

Nomenclature

D	Inner diameter of module [m]
Di	Inner diameter of hollow fiber [m]
Do	Outer diameter of hollow fiber [m]
L	Fiber length [m]
N	Number of fibers in the module
nc	Number of gas components
n	Number of internal collocation points
P	Feed side pressure [Pa]
p	Permeate side pressure [Pa]
Q_i	Permeance of component *i* [mol/(m^2 Pa s)]
R	Ideal gas constant [8.314 Pa m^3/(mol K)]
T	Temperature [K]
U	Feed-side flow rate [mol/s]
u_{xi}	Feed-side flow rate of component *i* [mol/s]
v	Permeate-side flow rate [mol/s]
v_{yi}	Permeate-side flow rate of component *i* [mol/s]
x_i	Feed-side concentration of component *i*
y_i	Permeate-side concentration of component *i*
z	Hollow fiber length variable [m]
μ_m	Dynamic viscosity of gas mixture [Pa s]

Subscripts

F	Feed
j,k	Index of collocation point
i	Index of component
p	Permeate
r	Retentate
swp	Sweep

UOP, Air Liquide, Cynara-NATCO) of membrane systems using different materials (cellulose acetate (CA) and polyimide (PI)) for CO_2 removal from natural gas were summarized by (He et al. (2013)). Among them, UOP implemented their spiral-wound module (Separex^{TM}) in natural gas field in offshore Malaysia in 2007. Cynara-NATCO installed a cellulose triacetate membrane system using 16 inch hollow fiber modules in Thailand (Bernardo et al., 2009). The CA membranes have some challenges in facing gas streams with high CO_2 partial pressures (beyond 10 bar) due to a significant plasticization effect (CO_2 acting as a partial solvent to the polymer causing overall higher permeances for all gases and lower selectivity) (Schell et al., 1989) at high pressure operation. The PI membrane performances are highly structure dependent, and the uncertainty regarding the influence of the exact chemical structure of commercial polyimides on the actual obtainable CO_2 permeance is still unknown. Moreover, PI membranes are well-known to be highly influenced by trace impurities of aromatics hydrocarbons (e.g., BTEX (benzene, toluene, ethylbenzene and xylenes)) in natural gas. Carbon membranes has the advantages of no/minor CO_2 plasticization due to the rigid structure, and no significant permeance decrease was found from the pure CO_2 permeation testing up to 50 bar (Haider et al., 2018). Cellulose derived carbon membranes were prepared by carbonization of cellulose-based precursors in the absence of oxygen to a final temperature in the range of 500 to 750 °C (He et al., 2011; He and Hägg, 2011; He and Hägg, 2012), and the CO_2/CH_4 selectivity can achieve >100 based on a molecular sieving transport mechanism (Haider et al., 2016), which is higher compared to the polymeric CA and PI membranes. However, carbon membranes have also challenges of being a brittle material woundable to shear stress fracturing and low tolerances to toluene in natural gas (Haider et al., 2018). Moreover, the durability of carbon materials towards the other BTEX are still unknown.

In addition to membrane material properties, membrane module design and process optimization play important roles in successful applications of membranes for gas separations (He et al., 2015; Favre, 2011). Considering the large-scale applications of hollow fiber membrane modules, the module efficiency is an important parameter for the design of cost-effective membrane system. It should be noted that determining concentration profiles and pressure drops along the length of specific dimension hollow fiber membranes is crucial for the design of efficient modules with maximized effective membrane area usage. Mathematical modeling has been reported to investigate gas transport through hollow fiber modules in literature (Pan, 1986; Kovvali et al., 1994; Coker et al., 1998; Tessendorf et al., 1999; Kaldis et al., 1998; Marriott and Sørensen, 2003; Peer et al., 2008; Shahsavand and Chenar, 2007). A good membrane model is required to predict membrane separation performance and provide valuable information for module design. The Pan's model is widely accepted as the most practical representation of multicomponent gas transport through high-flux asymmetric hollow fiber membranes (Pan, 1986). However, the model solution is based on a trial-and-error shooting method which requires initial estimates of pressure and concentration profiles along fiber length. In order to reduce the mathematical complexity and computational effort, different approaches (e.g., linear approximation (Kovvali et al., 1994), finite difference (Murad Chowdhury et al., 2005) and orthogonal collocation (Tessendorf et al., 1999; Kaldis et al., 1998; Kundu et al., 2013) have been proposed to solve the model. (Kovvali et al., 1994) presented a linear approximation model coupled with fourth-order Runge–Kutta and trapezoidal methods to solve multicomponent gas transport equations in a counter-current mode using the assumption of linearity between feed and permeate side composition. The assumption yields algebraic analytical expressions for prediction of membrane area and pressure ratio. Some researches in the literature (Tessendorf et al., 1999; Kaldis et al., 1998; Kundu et al., 2013; Kaldis et al., 2000) were reported to use the orthogonal collocation method to approximate nonlinear differential equations, which yields fewer algebraic equations to improve the solution accuracy. Moreover, it can also predict the profiles of basic variables (e.g., flow rate and concentration) along the fiber length at selected collocation points, which provides insight into the design of membrane modules. Thus, in this work, a membrane model considering pressure drops in both feed and permeate sides is developed to simulate gas transport through hollow fiber membrane modules based on the orthogonal collocation method. Moreover, the differential gas transport equations are described based on pressure and flow rate along the effective fiber length directly, and thus the computational complexity is significantly reduced. The developed membrane model was compared with different methods implemented in ChemBrane (in-house developed membrane model) and validated against experimental data, and then used for module design related to hollow fiber diameter and length as well as module packing density. Finally, the developed model was also applied for process parametric study of CO_2 removal from natural gas with different membranes.

2. Method

2.1. *Mathematical modeling*

The mathematical model developed in this work permits simulation of co-current and counter-current flow patterns with shell-side or bore-side feed. The following considerations and assumptions are applied in the membrane model (Mollocator):

1) Even though there is usually a cross flow mode near the ends of hollow fibers due to non-axial movement of the feed and permeate gases entering and exiting the bundle, the perfect counter-current (or co-current) flow patterns are still used to simplify the transport model.
2) The non-uniformity in the packing density of commercial hollow fiber modules may lead to different axial flows in local regions, and cause back mixing, radial flow, local bypassing and transportation along the wall on the shell side. However, the uniform axial flows are still considered in this model.

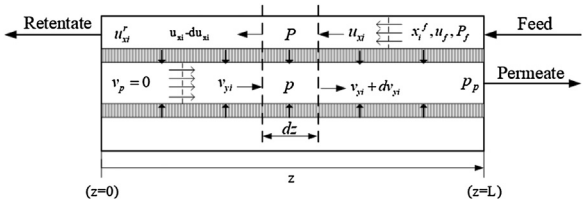

Fig. 1 – The counter-current flow pattern in a hollow fiber module without sweep gas.

3) Local Joule–Thomson effect with the permeation of significant amounts of CO_2 is ignored due to an expected high heat transfer coefficient of membrane materials reported in our previous work (He and Hägg, 2017). Thus, the whole system is assumed to be at isothermal conditions.
4) Gas flows in both feed and permeate side are in plug flow mode, and the radial velocity distribution is not taken into account.

The permeation of a multicomponent gas mixture through a hollow fiber membrane module in the counter-current flow patterns with shell-side feed is illustrated in Fig. 1, where the permeate flow direction is defined to be the positive z direction. The feed and permeate flow rates of gases through a differential element of membrane at length z are described by the Eqs. (1) and (2).

Feed side flow rate:

$$\frac{d(u_{xi})}{dz} = \pi D_o N Q_i \ (Px_i - py_i) \tag{1}$$

Permeate side flow rate:

$$\frac{d(v_{yi})}{dz} = \pi D_o N Q_i \ (Px_i - py_i) \tag{2}$$

The pressure drops in both sides of the differential element are calculated by the Eqs. (3) and (4), which are based on the derivation in Appendix A.

Feed side pressure drop:

$$\frac{dP}{dz} = \frac{192 N D_o (D + N D_o) R T \mu_m}{\pi (D^2 - N {D_o}^2)^3 P} u \tag{3}$$

Permeate side pressure drop:

$$\frac{dp}{dz} = -\frac{128 R T \mu_m}{\pi {D_i}^4 N p} v \tag{4}$$

The various flow rates and pressure drops in the feed and permeate sides operated with different flow patterns and module configurations (i.e., shell- or bore- side feed) are described in Table 1.

Relevant parameters in the Eqs. (1)–(4) are defined by the following equations:

$$u_{xi} = u x_i;\ v_{yi} = v y_i;\ u = \sum_{i=1}^{nc} u_{xi};\ v = \sum_{i=1}^{nc} v_{yi};$$

$$x_i = \frac{u_{xi}}{u};\ y_i = \frac{v_{yi}}{v} \ (v \neq 0) \tag{5}$$

In order to solve the differential equations, the following dimensionless variables are introduced:

$$z^* = \frac{z}{L},\ z^* \in [0,\ 1];\ {u_{xi}}^* = \frac{u_{xi}}{u_f};\ {v_{yi}}^* = \frac{v_{yi}}{u_f};\ P^* = \frac{P}{P_f};\ p^* = \frac{p}{P_f} \tag{6}$$

$$K_i = \frac{\pi D_o L N P_f Q_i}{u_f};\ K_{pu} = \frac{192 \mu_m R T N D_o (D + N D_o) L u_f}{\pi (D^2 - N {D_o}^2)^3 N {P_f}^2};$$

$$K_{pv} = \frac{128 \mu_m R T L u_f}{\pi {D_i}^4 N {P_f}^2} \tag{7}$$

By the substitution of Eqs. (6) and (7) into Eqs. (1)–(4), the dimensionless equations of Eqs. (8)–(11) for a multicomponent gas transport inside a counter-current and shell-side feed hollow fiber module can be obtained.

$$\frac{d({u_{xi}}^*)}{dz^*} = K_i \left(P^* \frac{{u_{xi}}^*}{\sum_{i=1}^{nc} {u_{xi}}^*} - p^* \frac{{v_{yi}}^*}{\sum_{i=1}^{nc} {v_{yi}}^*} \right) \tag{8}$$

$$\frac{d({v_{yi}}^*)}{dz^*} = K_i \left(P^* \frac{{u_{xi}}^*}{\sum_{i=1}^{nc} {u_{xi}}^*} - p^* \frac{{v_{yi}}^*}{\sum_{i=1}^{nc} {v_{yi}}^*} \right) \tag{9}$$

$$\frac{dP^*}{dz^*} = K_{pu} \frac{\sum_{i=1}^{nc} {u_{xi}}^*}{P^*} \tag{10}$$

$$\frac{dp^*}{dz^*} = -K_{pv} \frac{\sum_{i=1}^{nc} {v_{yi}}^*}{p^*} \tag{11}$$

Moreover, the boundary conditions is described as follows:

Feed entry:

$$at\ z^* = 1:\ {u_{xi}}^* = {u_f}^* x_f;\ P^* = {P_f}^*$$

Permeate without sweep gas

$$at\ z^* = 0:\ {v_{yi}}^* = 0$$

$$at\ z^* = 1:\ p^* = {p_p}^*$$

Permeate with sweep gas

$$at\ z^* = 0:\ {v_{yi}}^* = {v_{swp}}^* {y_{swp}};\ p^* = {p_{swp}}^*$$

It is worth noting that orthogonal collocation is a weighted residual method, which yields discrete approximations to first-order differential equations as:

$$\left(\frac{dw}{dz^*}\right)_{z_k^*} = \sum_{j=1}^{n+2} A_{k,j} w_j \tag{12}$$

where w is a given differential variable, k and j represents the index of collocation points, A is matrix of first derivative weights. By substituting differential terms with discrete

Table 1 – The descriptions of flow rates and pressure drops in feed and permeate side with different flow patterns and module configurations.

Flow pattern	Parameter	Shell-side feed	Bore-side feed
Counter-current	Feed side flow rate	$\frac{d(u_{xi})}{dz} = \pi D_o N Q_i\ (Px_i - py_i)$	$\frac{d(u_{xi})}{dz} = \pi D_o N Q_i\ (Px_i - py_i)$
	Permeate side flow rate	$\frac{d(v_{yi})}{dz} = \pi D_o N Q_i\ (Px_i - py_i)$	$\frac{d(v_{yi})}{dz} = \pi D_o N Q_i\ (Px_i - py_i)$
	Feed side pressure drop	$\frac{dP}{dz} = \frac{192 N D_o\,(D+N D_o) R T \mu m}{\pi (D^2 - N D_o^2)^3 P} u$	$\frac{dP}{dz} = \frac{128 R T \mu m}{\pi D_i^4 Np} u$
	Permeate side pressure drop	$\frac{dp}{dz} = -\frac{128 R T \mu m}{\pi D_i^4 Np} v$	$\frac{dp}{dz} = -\frac{192 N D_o\,(D+N D_o) R T \mu m}{\pi (D^2 - N D_o^2)^3 P} v$
Co-current	Feed side flow rate	$\frac{d(u_{xi})}{dz} = -\pi D_o N Q_i\ (Px_i - py_i)$	$\frac{d(u_{xi})}{dz} = -\pi D_o N Q_i\ (Px_i - py_i)$
	Permeate side flow rate	$\frac{d(v_{yi})}{dz} = \pi D_o N Q_i\ (Px_i - py_i)$	$\frac{d(v_{yi})}{dz} = \pi D_o N Q_i\ (Px_i - py_i)$
	Feed side pressure drop	$\frac{dP}{dz} = -\frac{192 N D_o\,(D+N D_o) R T \mu m}{\pi (D^2 - N D_o^2)^3 P} u$	$\frac{dP}{dz} = -\frac{128 R T \mu m}{\pi D_i^4 Np} u$
	Permeate side pressure drop	$\frac{dp}{dz} = -\frac{128 R T \mu m}{\pi D_i^4 Np} v$	$\frac{dp}{dz} = -\frac{192 N D_o\,(D+N D_o) R T \mu m}{\pi (D^2 - N D_o^2)^3 P} v$

approximations of Eq. (12), the Eqs. (8)–(11) can be reformulated as follows:

$$f_{k,i} = \sum_{j=1}^{n+2} A_{k,j} u_{j,xi}^{*} - K_i \left(P^{*} \frac{u_{xi}^{*}}{\sum_{i=1}^{nc} u_{xi}^{*}} - p^{*} \frac{v_{yi}^{*}}{\sum_{i=1}^{nc} v_{yi}^{*}} \right) = 0 \quad (14)$$

$$f_{k,i} = \sum_{j=1}^{n+2} A_{k,j} v_{j,yi}^{*} - K_i \left(P^{*} \frac{u_{xi}^{*}}{\sum_{i=1}^{nc} u_{xi}^{*}} - p^{*} \frac{v_{yi}^{*}}{\sum_{i=1}^{nc} v_{yi}^{*}} \right) = 0 \quad (15)$$

$$f_k = \sum_{j=1}^{n+2} A_{k,j} P_j^{*} - K_{pu} \frac{\sum_{i=1}^{nc} u_{xi}^{*}}{P^{*}} = 0 \quad (16)$$

$$f_k = \sum_{j=1}^{n+2} A_{k,j} p_j^{*} + K_{pv} \frac{\sum_{i=1}^{nc} v_{yi}^{*}}{p^{*}} = 0 \quad (17)$$

The Mollocator is programmed in Matlab, and the original model (a system of differential equations) is converted to a system of non-linear algebraic equations that is solved by Matlab fsolve (Optimization Toolbox) which is based on a Newton-Raphson type iteration scheme. The total number of the non-linear algebraic equations to be solved is 2(*nc*+1)(*n*+2), where *nc* is the number of chemical components transport through membrane and *n* is number of internal collocation points.

2.2. Model validation

The developed membrane model of Mollocator is validated by modelling of CO_2/CH_4 separation by three different types of modules. The Module A is designed with shell-side feed in a co-current flow pattern without sweep. The Module B is considered of a counter-current flow pattern for shell-side feed and bore-side permeate without sweep gas. The Module C is bore-side feed in a counter-current flow pattern with sweep gas. In total, five representative scenarios are investigated on different modules and operating conditions as listed in Table 2. A polyimide membrane was selected for the first three scenarios (1–3), and the gas permeabilities were taken from the work reported by (Nagel et al. (2002)). The simulation results from the Mollocator are compared respectively with the results simulated by the Runge–Kutta (Scenario 1) and successive stage method (Scenarios 2 and 3) implemented in ChemBrane (in-house membrane model (Grainger, 2007)). It should be noted that ChemBrane will only calculate the total membrane area without considering the specific module characteristics (e.g., hollow fiber dimension, packing density), and cannot calculate pressure drops inside membrane unit.

The Mollocator prediction results were also compared with the experimental data obtained from the gas permeation tests. For the Scenario 4, the pilot-scale hollow fiber carbon membrane module with the effective area of 2 m^2 was tested at 25 °C by feeding a 10 mol% CO_2 /90 mol% CH_4 premixed gas at 5 bar without sweep gas. The feed flow and pressure are controlled by mass flow controller and back pressure controller, respectively. The actual feed pressure was also recorded by the pressure transducers. The gas compositions in the permeate and retentate are analyzed by a gas chromatography (GC, 8610C, SRI Instruments Inc., USA). For the gas permeation measurements, the two most significant sources of experimental errors are the pressure transducers in feed side (Fuji Electric, France; Model FCX, range 0–120 bar) and the permeate flow measurements by a mass flow meter (Bronkhorst, Nederland; El-Flow series range 0–2.4 N L/min). While in the Scenario 5, a lab-scale module consisting of 106 hollow fiber carbon membranes was tested with a gas mixture of 40 mol% CO_2 /60 mol% CH_4 at 5 bar with the sweep gas of N_2 (He et al., 2018).

2.3. Module design parameter study

In order to design a high-efficiency hollow fiber module, great effort should be placed to achieve a high average driving force over the whole membrane area (Shao and Huang, 2006). From the Eqs. (3) and (4), it can be seen that pressure drops in shell- and bore-side are dependent on module design parameters of hollow fiber diameter and length, and packing density as well as process operating parameters such as pressure and gas velocity (determined by flow and cross-sectional area). It should be noted that feed and permeate flows are not the design variables, and operating pressure is dependent on the separation requirements and the selected membrane materials. Moreover, the membrane thickness is a material property, which is considered as a design parameter for developing high performance membranes, but not for the design of high efficiency modules. Therefore, it was not considered in this work as we are focusing on the investigation of module design parameters. Thus, particular attention was paid in this work

Table 2 – List of five different model validation scenarios.

Parameter	Scenario				
	1	2	3	4	5
Temperature (T) [K]	308	308	308	298	298
Feed pressure (P_f) [bar]	35	35	15	5	5
Permeate pressure (P_p) [bar]	1	1	1	1	1
Feed flow (u_f) [mol/s]	0.35	0.35	0.35	3.718×10^{-4}	4.464×10^{-4}
Sweep flow (v_s) [mol/s]	–	–	–	–	2.012×10^{-5}
Feed CO_2 composition (x_f) [mol%]	10	10	10	10	40
Feed CH_4 composition (x_f) [mol%]	90	90	90	90	60
CO_2 Permeance [10^{-9} mol/(m^2 Pa s)]	3.207	3.207	3.207	1.749	8.405
CH_4 Permeance [10^{-10} mol/(m^2 Pa s)]	1.33	1.33	1.33	1.227	1.323
N_2 Permeance [10^{-10} mol/(m^2 Pa s)]	–	–	–	–	3.968
Inner diameter of module (D) [m]	0.1	0.1	0.05	0.024	0.012
Outer diameter of fiber (D_o) [μm]	250	250	170	180	200
Inner diameter of fiber (D_i) [μm]	200	200	120	126	150
Fiber length (L) [m]	0.6	0.6	1.5	0.8	0.3
Number of fibers (N)	60,000	60,000	60,000	2805	106
Membrane material	Polyimide	Polyimide	Polyimide	Carbon	Carbon
Packing density [m^2/m^3]	6000	6000	16,300	3510	590
Module type	A	B	B	B	C

Table 3 – Different simulation scenarios for module design.

Scenario	Hollow fiber inner diameter [μm]	Hollow fiber outer diameter [μm]	Hollow fiber length [m]	Number of fibers [N]	Packing density [m^2/m^3]	Module inner diameter [m]
A	100–300	150–350	0.6	Adjust accordingly	6000	0.1
B	150–200	200–250	0.5-2	Adjust accordingly	6000	Adjust accordingly
C	200	250	0.6	60,000	6000–14,250	Adjust accordingly

to investigate the influences of module design parameters on module efficiency. Three simulation scenarios listed in Table 3 were conducted with a constant membrane area under a given operation condition (Scenario 2 in Table 2). The hollow fiber inner diameter of 100–300 μm, the fiber length of 0.5–2 m and the module packing density of 6000 m^2/m^3 are chosen based on the knowledge from commercial membrane modules.

2.4. *Process simulation*

CO_2 content in raw natural gas is dependent on the gas fields and will usually increase as time passes (Chu and He, 2018). The typical natural gas contains 10% CO_2 and 90% hydrocarbons (C1–C4) together with impurities of heavy hydrocarbons, H_2O and H_2S. The dehydrated (dry) natural gas is simulated to simplify the simulation. Membrane system was reported for water dehydration before the acid gas removal (Lin et al., 2013). Thus, water permeation is not considered in this work as we assumed dry natural gas is fed into the system. High content of CO_2 should be taken out from raw natural gas to reach the pipeline specification, which is varying to some extent depending on gas quality demands in different countries. Membrane system shows great potential for natural gas sweetening due to the advantages of being small footprint, low capital and operating costs. It is worth noting that membrane unit modeling is crucial to document technology feasibility in a precise way based on process simulation. Thus, it is interesting to optimize process parameters of membrane system for natural gas sweetening.

Three different hollow fiber membranes (i.e., cellulose acetate (CA) and polyimide (PI) and cellulose derived carbon membranes) are used for modeling of CO_2 removal from natural gas. The CO_2 permeance of the PI membranes is estimated to 3.283×10^{-8} mol/(m^2 Pa s), and the other gas permeances are taken or estimated from the literature (Baker, 2002; Koros and Mahajan, 2000). Carbon membrane performance is taken from the work reported by Haider et al. (2016). The gas permeation data of different membranes for natural gas sweetening are listed in Table 4, which are used as the simulation input. Moreover, the following basis and adaptions are applied to all the simulation scenarios for process parametric study:

1 The membrane operating temperature is 30 °C, and the permeate pressure is 1 bar;
2 The feed flow rate is 50 kmol/h;
3 The outer and inner diameter of hollow fibers are 200 μm and 150 μm, respectively. The hollow fiber length is 1 m;
4 Dehydrated (dry) natural gas with 1 mol% N_2 is simulated, and higher hydrocarbons (beyond propane) are ignored. The reason for not considering the higher hydrogen carbon is mainly due to the lack of experimental data of the gas permeances. However, it should be noted that carbon membranes studied in this work are based on the molecular sieving transport mechanism. The hydrocarbons of >C4 have larger kinetic diameters, and are expected to have very low gas permeance. Thus, all the hydrocarbons of > C4 are considered in C3;
5 The pipeline specification of 2.5 mol% of CO_2 is given according to gas quality requirement in many European countries (e.g., Norway, France, UK, and Denmark).

Based on the above assumptions and basis, seven scenarios with different operating parameters (including feed composition, pressure) are listed in Table 4, and the simulation of each scenario is conducted by the developed membrane model Mollocator. The required membrane area is optimized to achieve the 2.5 mol% CO_2 in the retentate, and the number of hollow fibers was calculated based on the membrane area and

Table 4 – List of simulation basis.

Scenario	Feed gas composition [mol%]					Feed Pressure (Pf) [bar]
	CO2	Methane	Ethane	Propane	N2	
1	5.0	81.7	8.2	4.1	1.0	60
2	10.0	77.4	7.7	3.9	1.0	60
3	20.0	68.7	6.9	3.4	1.0	60
4	30.0	60.0	6.0	3.0	1.0	60
5	40.0	51.3	5.1	2.6	1.0	60
6	50.0	42.6	4.3	2.1	1.0	60
7	10.0	77.4	7.7	3.9	1.0	40-100
Membrane	Gas permeance [mol/(m^2 Pa s)]					
CA (Schell et al., 1989; Baker, 2002; Bhide and Stern, 1993)	1.691×10^{-8}	1.127×10^{-9}	3.758×10^{-10}	3.381×10^{-10}	1.127×10^{-9}	
PI (Baker, 2002; Koros and Mahajan, 2000)	3.283×10^{-8}	1.641×10^{-9}	1.094×10^{-9}	5.469×10^{-10}	3.283×10^{-9}	
Carbon (Haider et al., 2016)	3.382×10^{-9}	3.382×10^{-11}	1.353×10^{-11}[a]	1.691×10^{-13}[a]	1.353×10^{-10}	

[a] Estimated from kinetic diameter of gas molecules.

the given fiber diameter and length. The cross-sectional area of membrane module housing is set to be twice of the total cross-sectional area for the hollow fibers-this is used to calculate the inner diameter of a module. In order to document the separation performance of different membrane systems, two important variables are considered. One is specific membrane area (defined as the ratio of the total required membrane area and feed flow rate, m^2/(kmol/h)), and the other is hydrocarbon (HC) loss in permeate (defined as the ratio of amount of hydrocarbon in permeate gas and amount of hydrocarbon in feed gas). The influences of process parameters (mainly CO_2 content in feed gas and feed pressure) on membrane separation performance are investigated.

3. Results and discussion

3.1. *Validation of mollocator*

The modeling results from Mollocator are very close to those simulated from ChemBrane as shown in Table 5, which is mainly due to the very small pressure drops in both feed and permeate sides (<10 mbar) for these two scenarios (Scenarios 1 & 2 in Table 2). The relative deviation (RD) (defined as: $RD = \frac{(x_{Mollocator} - x_{ChemBrane})}{x_{ChemBrane}} \times 100\%$) of the flow rates and compositions in both permeate and retentate are all <1%, which indicates that the Mollocator can be used for modeling gas transport behavior through hollow fiber membranes. However, the deviations of the simulation results between the two models is found to be larger (when pressure drops in both shell and bore side are higher for the Scenario 3 due to the applied higher packing density module and hollow fibers with smaller inner diameter. It is worth noting that ChemBrane does not calculate pressure drops on both membrane sides, and thus it has a significant difference of 11% in the permeate flow predicted from these two model. The Mollocator potentially provides a more accurate prediction of the gas transport behavior inside a module with high packing density (e.g., 16,300 m^2/m^3 in the Scenario 3) and highly permeable and small inner diameter (120 μm) hollow fiber membranes.

The simulation results from Mollocator was also compared with the experimental data. For the shell-side feed without sweep gas (Scenario 4), the Mollocator shows slightly lower permeate flow and permeate CO_2 purity compared to the experimental data. While for the bore-side feed with sweep gas (Scenario 5), the Mollocator predicts slightly relatively higher permeate flow and permeate CO_2 purity. However, the deviation between the Mollocator prediction and the experimental data ($RD = \frac{(x_{Mollocator} - x_{exp.})}{x_{exp.}} \times 100\%$) is less 5%, which indicates that the developed membrane model can predict gas transportation through hollow fiber membranes quite well (It should be noted that the combined experimental error for these instruments is expected to be in the range of 5%).

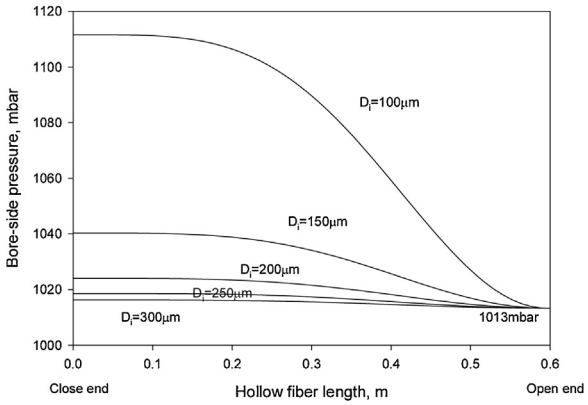

Fig. 2 – The influence of hollow fiber inner diameter on the bore-side pressure drop along fiber length (L = 0.6 m).

3.2. *Membrane module parameter study*

3.2.1. *Hollow fiber diameter design*

The influence of hollow fiber diameter on module efficiency was investigated by varying the hollow fiber inner diameter from 100 to 300 μm. By keeping a constant overall fiber thickness of 25 μm, the outer diameter of hollow fibers is changed from 150 to 350 μm accordingly. The modeling was conducted based on the Scenario A from Table 3 by using a fixed packing density of 6000 m^2/m^3, and the results are shown in Fig. 2. Significant bore-side pressure drops along the fiber length are found for the modules with smaller inner-diameter hollow fibers as pressure drop is inversely proportional to D_i^4 based on the Eq. (4). It can be found that modules with larger hollow fibers have lower bore-side pressure drop and higher driving force efficiency. When the fiber inner diameter is larger than 200 μm, the total pressure drop along the length is less than 1%, which is acceptable in most applications. Further reducing the hollow fiber diameter can dramatically cause the increase of pressure drop in the permeate side, which

Table 5 – Comparison of Mollocator with ChemBrane and experimental data.

Scenario	Source	Permeate flow [mol/s]	Permeate CO_2 purity [mol%]	Retentate flow [mol/s]	Retentate CH_4 purity [mol%]
1	ChemBrane	0.03	59.12	0.32	94.77
	Mollocator	0.0298	59.54	0.3202	94.60
	RD [%]	−0.67	0.71	0.06	−0.18
2	ChemBrane	0.03	59.88	0.32	94.94
	Mollocator	0.0303	60.34	0.3197	94.77
	RD [%]	1.00	0.77	−0.09	−0.18
3	ChemBrane	0.0205	56.72	0.3294	92.92
	Mollocator	0.0181	56.04	0.3319	92.52
	RD [%]	−11.71	−1.20	0.76	−0.43
4	Experimental	4.313×10^{-5}	25.96	3.287×10^{-4}	92.09
	Mollocator	4.258×10^{-5}	25.04	3.292×10^{-4}	91.95
	RD [%]	−1.28	−3.54	0.15	−0.15
5	Experimental (He et al., 2018)	4.464×10^{-5}	54.40	4.219×10^{-4}	63.30
	Mollocator	4.567×10^{-5}	55.37	4.209×10^{-4}	63.45
	RD [%]	2.31	1.78	−0.25	0.24

may significantly decrease the transport driving force of fast-gas component (i.e., CO_2) because of the increased gas partial pressure in the bore side. It should be noted that shell-side pressure drop is negligible due to a relatively low packing density of 6000 m^2/m^3 and a low simulated feed flow in this scenario.

3.2.2. *Hollow fiber length design*

The influence of hollow fiber length (*L*) on module performance was conducted by varying the fiber length from 0.5 to 2 m, and the simulations were performed based on the Scenario B given in Table 3. The results are shown in Fig. 3. It can be seen that there is a slight effect of hollow fiber length on the actual module performance related to CH_4 purity and CH_4 loss for the simulated membranes at a given constant area. Increasing the hollow fiber length causes the reductions of the retentate CH_4 purity and the CH_4 loss. It should be noted the overall difference is very small between the short-big module (similar to several modules in parallel operation) and the long-slim module (like several modules in series operation), which means the modules operated in series or parallel has minor difference in this study. However, one should expect that modules with high-selectivity membranes (e.g., carbon membranes) may present a relatively large difference-this should be further investigated in future work.

3.2.3. *Packing density design*

The influence of module packing density on module performance was conducted by varying the packing density from 6000 to 14,250 m^2/m^3 with constant fiber diameter, length and membrane surface area. The simulations were performed based on the Scenario C given in Table 4. At a given feed flow in the shell side, the modules with higher packing densities present higher pressure drops due to the smaller cross-sectional areas in the shell side (i.e., higher gas velocity in Eq. (3)) as shown in Fig. 4. Therefore, reducing module packing density can potentially enhance the overall module efficiency, but, the footprint of the membrane modules increases with the increase of the module inner diameter as shown in Fig. 4(b), which should also be taken into account for membrane module/system design, especially if intended usage is an off-shore platform. It should also be noted that the highest module packing density depends on hollow fiber dimension. In this work, the module packing density of 14,250 m^2/m^3 is found to be the maximum using the hollow fibers with the outer diameter of 250 μm, and further increasing packing density will cause extreme high pressure drops or not be possible for making any realistic module.

3.3. *Process and feed-specification parametric study*

3.3.1. *Concentration and pressure profiles*

The calculated gas concentration profiles and the pressure drops along fiber length in the feed and permeate side operated in the counter-current mode are shown in Fig. 5, which are simulated with a 10 mol% CO_2 content natural gas feeding from shell-side at a feed pressure of 60 bar (the Scenario 2 in Table 4). The efficiency of membrane area usage along the fiber length is different, and the close-end section presents a lower driving force compared to the open-end section as shown in Fig. 5(a) and (b). It is worth noting that a very small pressure drop (the maximum of 106 mbar for the PI membranes (<0.15%) over the whole fiber length) was found on the shell side due to the relatively low packing density module operated at a low feed flow (i.e., very low gas velocity) as shown in Fig. 5(a). However, significant pressure drops in the bore side were found for all the three membranes due to the small hollow fiber inner diameters, especially the highly permeable PI membranes with a high permeate flow (i.e., pressure drop is dependent on gas velocity). Moreover, for the same membrane area, the carbon membranes produce higher purity CO_2 in the permeate with single-stage membrane system as shown in Fig. 5(c). The PI and CA membranes present higher permeate CH_4 flow (i.e., higher CH_4 loss) due to the lower CO_2/CH_4 selectivities as indicated in Fig. 5(d). Therefore, multi-stage systems for the PI and CA membranes are required to achieve low CH_4 loss and high purity CO_2 in permeate (potentially used for enhanced oil/gas recovery).

3.3.2. *Feed CO_2 content influence*

The sensitivity analysis of feed CO_2 content on membrane module performance was conducted for the scenarios 1–6 of Table 4. Fig. 6(a) shows that the required specific membrane area increases with the increase of CO_2 content in feed gas, but slightly decreases at >35 mol%. The influence of feed CO_2 content on the specific required area for the carbon membranes is more significant compared to the other two types of membranes. The HC loss increases with the increase of feed CO_2 content as shown in Fig. 6(b), but the carbon membrane shows a much lower HC loss. These results indicate that a single-

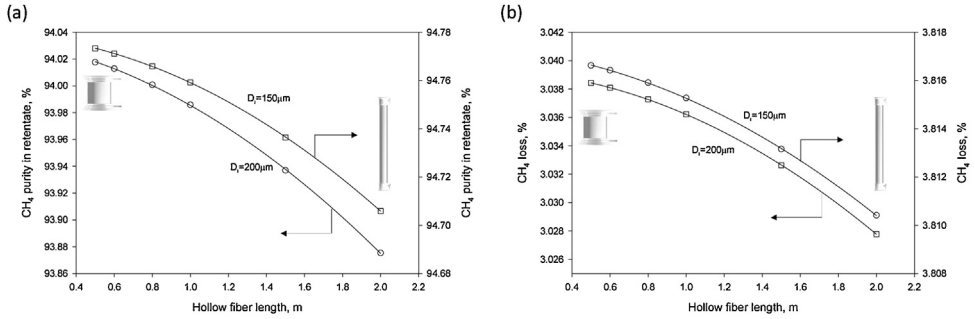

Fig. 3 – The influence of hollow fiber length on CH_4 purity in retentate (a) and CH_4 loss in permeate (b) with different fiber inner diameters.

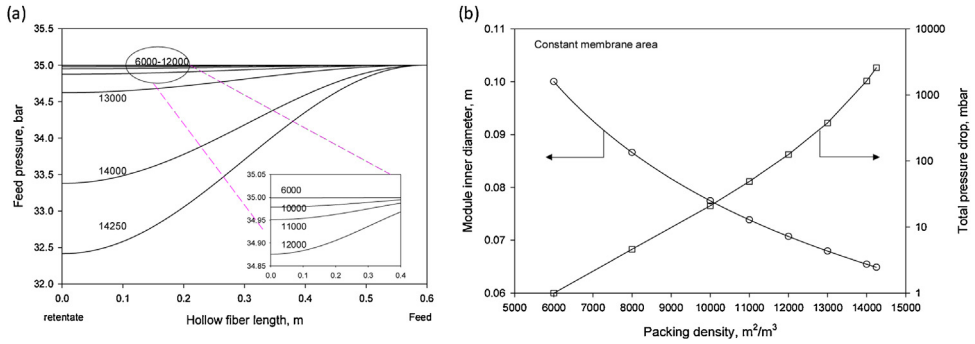

Fig. 4 – The feed pressure profiles along the fiber length for the modules (a) and the module inner diameter and total pressure drop (b) with different packing densities.

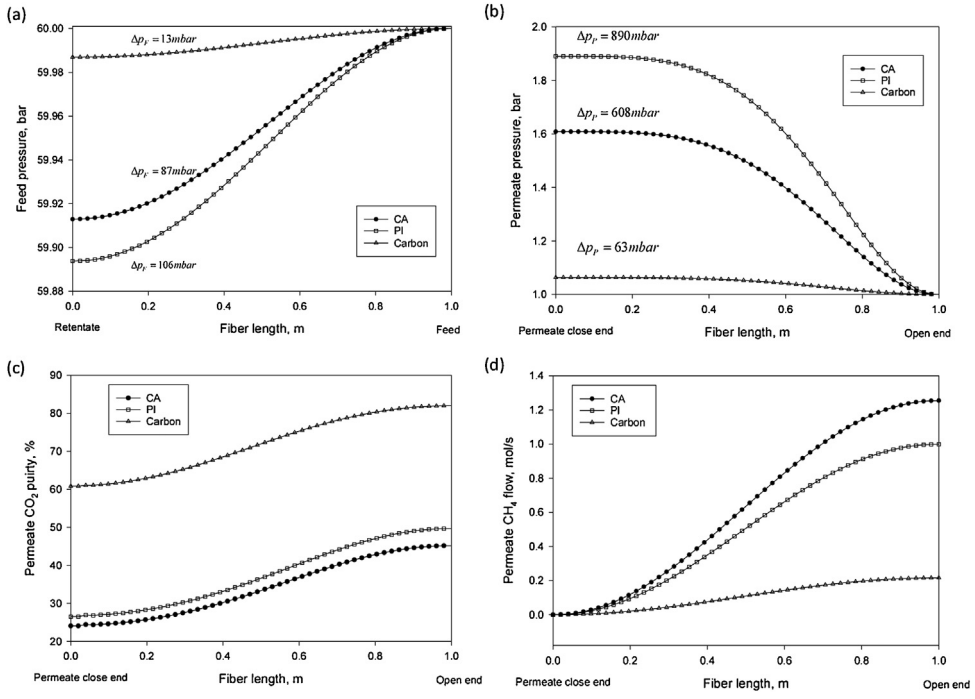

Fig. 5 – Feed pressure drop in the shell side (a), permeate pressure drop in the bore side (b), CO_2 concentration profiles (c) and permeate CH_4 flow profiles (d) along hollow fiber length with the fiber inner diameter of 150 μm.

stage polymeric (CA or PI) membrane system (with CO_2/CH_4 selectivity <30 given in Table 4) is usually quite challenging to achieve low HC loss (e.g., <2% required in most gas plants). In order to reduce the HC loss of CA and PI membranes, a multi-stage membrane system is required, but this will increase energy consumption and required membrane area. The details of this is however not included in this work. Moreover, the module inner diameter increases with the increase of the feed CO_2 content up to 30% as shown in Fig. 6(c). Further increasing feed CO_2 content will not influence the required membrane area, and thus no changes in the module inner diameter, which is mainly due to the negligible partial pressure in the permeate compared to the high partial pressure in the feed (i.e., $\frac{p_{P,i}}{p_{F,i}} < 5\%$) when feed CO_2 concentration is higher than 30 mol%.

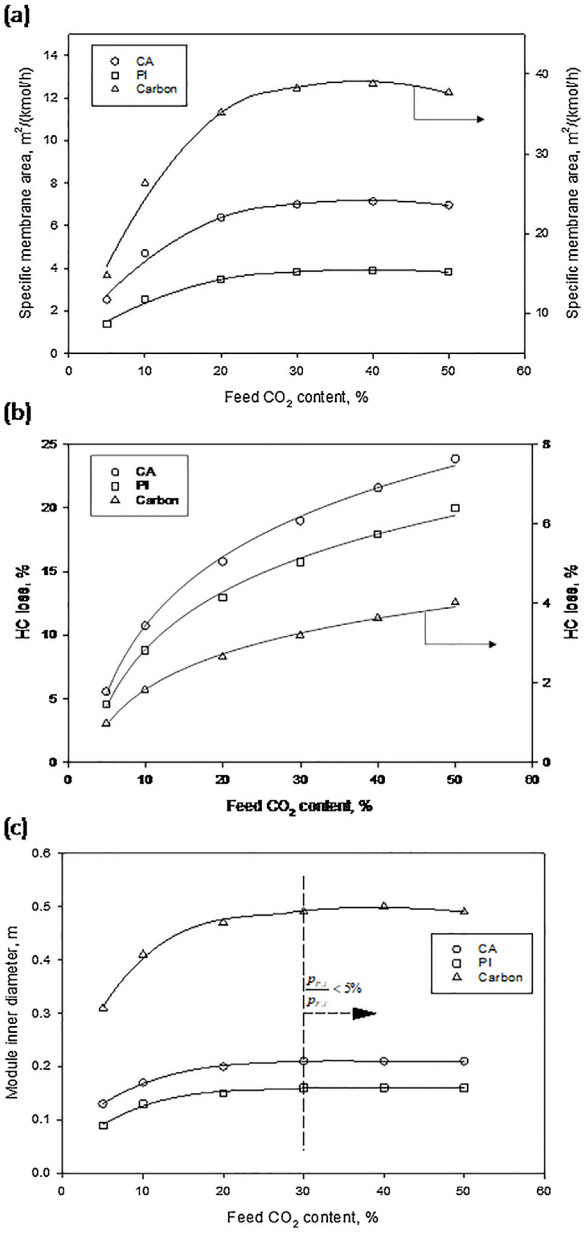

Fig. 6 – The influence of CO_2 content in feed gas on specific membrane area (a), HC loss (b), and the required module inner diameter (c).

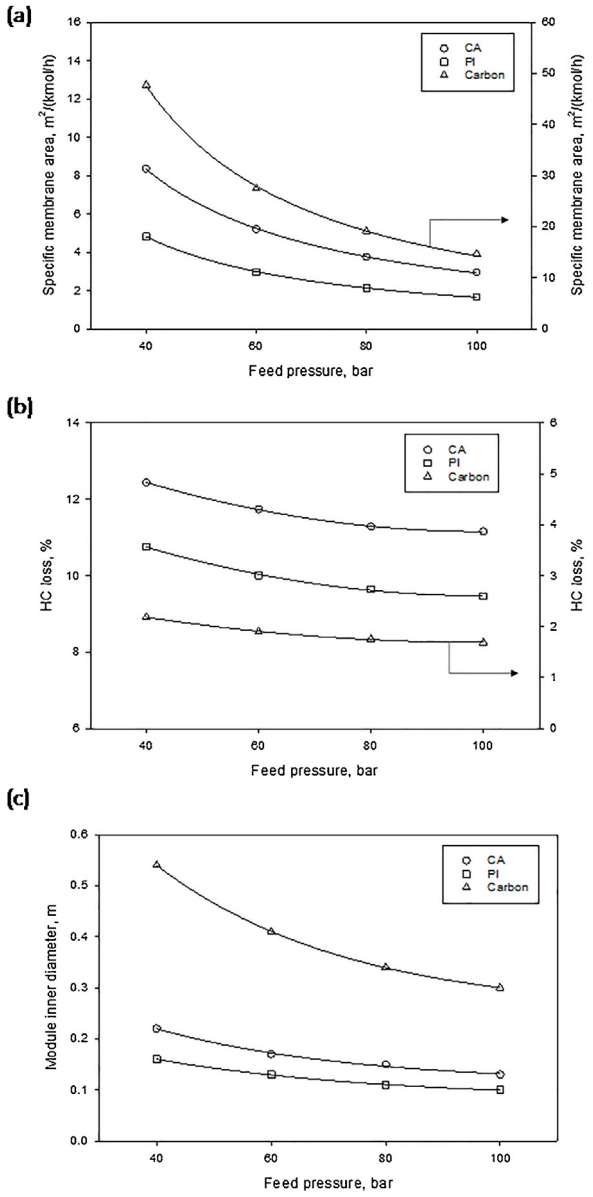

Fig. 7 – The influence of feed gas pressure on specific membrane area (a), hydrocarbon loss (b) and the required module inner diameter (c).

3.3.3. *Feed pressure influence*

Feed pressure variation from 40 to 100 bar were simulated using the developed Mollocator model for the simulation of the scenario 7 listed in Table 4, and the results are shown in Fig. 7. It can be seen that required specific membrane area and HC loss decrease with the increase of feed gas pressure (Fig. 7(a) and (b)). It is also found that larger carbon membrane area (due to a low gas permeance given in Table 4) is required compared to the other two membranes, but the HC loss (<2%) is much lower due to the higher CO_2/CH_4 selectivity. However, the module footprint (related to module inner diameter) of carbon membrane is much larger, which decreases with the increase of feed pressure as shown in Fig. 7(c). It should be noted that the raw natural gas pressure is usually unchangeable in a specific gas plant, then the selection of the right membrane materials as well as the optimization of other process parameters will be essential. Thus, future work on cost minimization should be conducted to identify the optimal process conditions for the specific membrane materials.

3.4. *Future perspectives*

It should be noted that the focus of this work is the efficient module design and process/field specific parametric study of CO_2 removal from natural gas based on the developed membrane simulator (Mollocator). The HC loss and required membrane area as well as the detailed cost estimation are not included in the simulated scenarios. Generally, a reduction in the specific membrane area is approximately proportional to a reduction of membrane unit cost (He et al., 2014). Whereas, a reduction in HC loss means that operating cost will be lower. Therefore, it is obvious that the PI materials performs better than CA membranes on both required membrane area and HC loss for all feed loadings. However, the comparison between the PI membranes and the carbon membranes is not so straight forward. The carbon membranes will most likely be more expensive due to the larger required membrane area and the higher material production cost (He and Hägg, 2013), but the reduction in HC loss is significant and may offset the incremental installation cost by reducing operating cost. If a

process based on polymeric membranes is to yield a comparable hydrocarbon loss, then a multi-stage membrane process is needed, and this will introduce additional compressors and require more membrane area. Therefore, future work on integration of the Mollocator into Aspen HYSYS via Cape-Open for process optimization can be conducted to identify the best membrane material and process condition for natural gas sweetening.

4. Conclusions

A mathematical model, solved with the use of the orthogonal collocation method, is developed to simulate multicomponent gas separation by hollow fiber membrane modules. The developed Mollocator model permits simulation of co-current, counter-current flow patterns with or without sweep gas. Moreover, the developed model enables the predictions of flow rate, concentration and pressure profiles along fiber length in both feed and permeate to give a full insight into the multicomponent gas transport in a shell- or bore-side feed module. Validation against experimental data shows a minor deviation of less than 5% which is well within the expected experimental errors. It was even found that the deviation between the developed Mollocator model and ChemBrane can be quite small of <1% if pressure drops inside module are very low. However, the deviation can be significant (e.g., 11% in permeate flow) for the modules with a high packing density and small hollow fibers, which indicates that the developed Mollcator is superior to ChemBrane. Moreover, the developed membrane model can be used for hollow fiber module design with regarding to hollow fiber diameter and length as well as module packing density. The bore-side pressure drop is higher for the hollow fibers with smaller inner diameter, but it can be less 1% if the fiber inner diameter is larger than 200 μm. Moreover, increasing module packing density may cause a dramatic increase of pressure drop in the shell side, and thus appropriate packing density should be chosen to balance module performance and cost. Finally, the developed Mollocator model was successfully employed to investigate the influences of process parameters on natural gas sweetening with different membranes. Higher feed CO_2 concentration in natural gas increases the required membrane area and HC loss. Moreover, high feed pressure reduces the specific require membrane area and HC loss, but the operating cost related to power consumption increases. Thus, cost minimization should be further conducted to identify the optimal operating condition in the future work.

Funding

This work was supported by the Research Council of Norway (Norges forskningsråd, 267615).

Acknowledgements

The authors acknowledge the Research Council of Norway (Norges forskningsråd) for funding this work in the CO2Hing project (#267615) through the Petromaks2 programme. We also thank the discussions and comments with the project partners of the Institute of Process Engineering-Chinese Academy of Sciences, SINTEF AS and National Center of Scientific Research "Demokritos". Dr. Mohammad Ostadi is thanked for the recipe of integration of Matlab code into HYSYS via Cape-Open. The typical natural gas composition at well head as provided by Equinor is also acknowledged.

Appendix A

Eqs. (3) and (4) are obtained based on the following derivations:

$$P = \frac{F}{S}; F = AKC_f; K = \frac{1}{2}\rho\vartheta^2; \vartheta = \frac{Q}{S} \tag{A1}$$

where P is pressure, F force; A surface area, S cross-sectional area, K kinetic energy, C_f friction coefficient, ϑ velocity, ρ gas density, Q volume flow rate.

Shell side (Mulder, 1996)

$$A = \pi DL + N\pi D_o L; C_f = \frac{24}{Re}; Re = \frac{\rho\vartheta D_h}{\mu_m}; D_h = 4\frac{\frac{\pi D^2}{4N} - \frac{\pi {D_o}^2}{4}}{\pi D_o};$$
$$Q = \frac{uRT}{P}; S = \frac{\pi}{4}D^2 - N\frac{\pi}{4}{D_o}^2 \tag{A2}$$

$$\frac{dP}{dz} = \frac{192ND_o(D + ND_o)\mu_m RT}{\pi(D^2 - N{D_o}^2)^3 P}u \tag{A3}$$

Bore side (Mulder, 1996)

$$A = N\pi D_i L; C_f = \frac{16}{Re}; Re = \frac{\rho\vartheta D_i}{\mu_m}; Q = \frac{vRT}{P}; S = N\frac{\pi}{4}{D_i}^2 \tag{A4}$$

$$\frac{dp}{dz} = \frac{128\mu_m RT}{N\pi {D_i}^4 p}v \tag{A5}$$

where Re is Reynolds number, μ_m dynamic viscosity of gas mixture; D_h hydraulic diameter (assuming fibers arranged in a square pitch mode (He et al., 2017)).

References

Baker, R.W., 2002. Future directions of membrane gas separation technology. Ind. Eng. Chem. Res. 41 (6), 1393–1411.

Baker, R.W., Lokhandwala, K., 2008. Natural gas processing with membranes: an overview. Ind. Eng. Chem. Res. 47 (7), 2109–2121.

Bernardo, P., Drioli, E., 2010. Membrane gas separation progresses for process intensification strategy in the petrochemical industry. Pet. Chem. 50 (4), 271–282.

Bernardo, P., Drioli, E., Golemme, G., 2009. Membrane gas separation: a Review/State of the art. Ind. Eng. Chem. Res. 48 (10), 4638–4663.

Bhide, B.D., Stern, S.A., 1993. Membrane processes for the removal of acid gases from natural gas. I. Process configurations and optimization of operating conditions. J. Membr. Sci. 81 (3), 209–237.

Chu, Y., He, X., 2018. Process simulation and cost evaluation of carbon membranes for CO2 removal from high-pressure natural gas. Membranes 8 (4), 118.

Coker, D.T., Freeman, B.D., Fleming, G.K., 1998. Modeling multicomponent gas separation using hollow-fiber membrane contactors. AIChE J. 44 (6), 1289–1302.

Favre, E., 2011. Membrane processes and postcombustion carbon dioxide capture: challenges and prospects. Chem. Eng. J. 171 (3), 782–793.

Grainger, D.R., 2007. A simple method for solving mixed-permeate and counter-current membrane models with multi-component feeds. In: Doctoral Thesis Appendix.

Haider, S., Lindbråthen, A., Hägg, M.-B., 2016. Techno-economical evaluation of membrane based biogas upgrading system: a

comparison between polymeric membrane and carbon membrane technology. Green Energy Environ. 1 (3), 222–234.
Haider, S., et al., 2018. CO_2 separation with carbon membranes in high pressure and elevated temperature applications. Sep. Purif. Technol. 190, 177–189.
He, X., 2018. A review of material development in the field of carbon capture and the application of membrane-based processes in power plants and energy-intensive industries. Energy Sustain. Soc. 8 (1), 34.
He, X., Hägg, M.-B., 2011. Hollow fiber carbon membranes: investigations for CO_2 capture. J. Membr. Sci. 378 (1–2), 1–9.
He, X., Hägg, M.-B., 2012. Structural, kinetic and performance characterization of hollow fiber carbon membranes. J. Membr. Sci. 390-391, 23–31.
He, X., Hägg, M.-B., 2013. Hollow fiber carbon membranes: from material to application. Chem. Eng. J. 215–216, 440–448.
He, X., Hägg, M.-B., 2017. Investigation on nanocomposite membranes for high pressure CO_2/CH_4 separation. J. Membr. Sci. Technol. 7, 169.
He, X., et al., 2011. Preparation and characterization of hollow fiber carbon membranes from cellulose acetate precursors. Ind. Eng. Chem. Res. 50 (4), 2080–2087.
He, X., Yu, Q., Hägg, M.-B., 2013. CO_2 capture. In: Hoek, E.M.V., Tarabara, V.V. (Eds.), Encyclopedia of Membrane Science and Technology. John Wiley & Sons, Inc.
He, X., Hägg, M.-B., Kim, T.-J., 2014. Hybrid FSC membrane for CO_2 removal from natural gas: Experimental, process simulation, and economic feasibility analysis. AIChE J. 60 (12), 4174–4184.
He, X., Fu, C., Hägg, M.-B., 2015. Membrane system design and process feasibility analysis for CO2 capture from flue gas with a fixed-site-carrier membrane. Chem. Eng. J. 268, 1–9.
He, X., et al., 2017. Pilot testing on fixed-site-carrier membranes for CO_2 capture from flue gas. Int. J. Greenh. Gas Control 6, 323–332.
He, X., et al., 2018. Carbon molecular sieve membranes for biogas upgrading: techno-economic feasibility analysis. J. Clean. Prod. 194, 584–593.
Kaldis, S.P., et al., 1998. Simulation of binary gas separation in hollow fiber asymmetric membranes by orthogonal collocation. J. Membr. Sci. 142 (1), 43–59.
Kaldis, S.P., Kapantaidakis, G.C., Sakellaropoulos, G.P., 2000. Simulation of multicomponent gas separation in a hollow fiber membrane by orthogonal collocation — hydrogen recovery from refinery gases. J. Membr. Sci. 173 (1), 61–71.
Koros, W.J., Mahajan, R., 2000. Pushing the limits on possibilities for large scale gas separation: which strategies? J. Membr. Sci. 175 (2), 181–196.
Kovvali, A.S., Vemury, S., Admassu, W., 1994. Modeling of multicomponent countercurrent gas permeators. Ind. Eng. Chem. Res. 33 (4), 896–903.
Kundu, P.K., Chakma, A., Feng, X., 2013. Modelling of multicomponent gas separation with asymmetric hollow fibre membranes—methane enrichment from biogas. Can. J. Chem. Eng. 91 (6), 1092–1102.
Lin, H., et al., 2013. Dehydration of natural gas using membranes. Part II: sweep/countercurrent design and field test. J. Membr. Sci. 432, 106–114.
Marriott, J., Sørensen, E., 2003. A general approach to modelling membrane modules. Chem. Eng. Sci. 58 (22), 975–4990.
Mulder, M., 1996. Basic Principles of Membrane Technology, 2nd Ed., pp. 496–498.
Murad Chowdhury, M.H., et al., 2005. A new numerical approach for a detailed multicomponent gas separation membrane model and AspenPlus simulation. Chem. Eng. Technol. 28 (7), 773–782.
Nagel, C., et al., 2002. Free volume and transport properties in highly selective polymer membranes. Macromolecules 35 (6), 2071–2077.
Pan, C.Y., 1986. Gas separation by high-flux, asymmetric hollow-fiber membrane. AIChE J. 32 (12), 020–2027.
Peer, M., Mahdyarfar, M., Mohammadi, T., 2008. Evaluation of a mathematical model using experimental data and artificial neural network for prediction of gas separation. J. Nat. Gas Chem. 17 (2), 135–141.
Peters, L., et al., 2011. CO2 removal from natural gas by employing amine absorption and membrane technology—a technical and economical analysis. Chem. Eng. J. 172 (2–3), 952–960.
Schell, W.J., et al., 1989. Recent advances in cellulosic membranes for gas separation and pervaporation. Gas Sep. Purif. 3 (4), 162–169.
Shahsavand, A., Chenar, M.P., 2007. Neural networks modeling of hollow fiber membrane processes. J. Membr. Sci. 297 (1–2), 59–73.
Shao, P., Huang, R.Y.M., 2006. An analytical approach to the gas pressure drop in hollow fiber membranes. J. Membr. Sci. 271 (1), 69–76.
Tessendorf, S., Gani, R., Michelsen, M.L., 1999. Modeling, simulation and optimization of membrane-based gas separation systems. Chem. Eng. Sci. 54 (7), 943–955.